Journal of Applied Polymer Science

Electrospun dendritic ZnO nanofibers and its photocatalysis application

Jianing Li,[1] Zhiqiang Cheng,[1,2] Mengzhu Liu,[1] Mingyue Zhang,[1] Meijuan Hu,[1] Li Zhang,[1] Haifeng Jiang,[1] Junfeng Li[1]

[1]College of Chemistry, Jilin University, Changchun 130012, People's Republic of China

[2]College of Resources and Environment, Jilin Agriculture University, Changchun 130118, People's Republic of China

Correspondence to: J. Li (E-mail: jfli@jlu.edu.cn)

ABSTRACT: A simple and efficient procedure has been developed to fabricate ZnO nanofibers with dendritic structure via electrospinning and subsequent calcination. The spinning solution is prepared by mixing polyvinylpyrrolidone (PVP) and zinc acetate into methanol. From SEM images, it can be observed that the ZnO product has a tendency of dendritic structure. The diameter of the dendritic branch is ~137 nm. The structure and physicochemical property of the prepared nanofibers are elucidated by TGA, SEM, XRD, FTIR, and PL, respectively. The photoluminescene measurement of the ZnO samples exhibit a broad visible emission band concentrate on around 430–580 nm. Meanwhile, the intensity is related to the content of surface oxygen vacancies, which probably influence photocatalytic activity of ZnO samples. Whereafter, the photocatalytical activity of the ZnO nanofibers is evaluated by quantifying the degradation of methyl blue. The result indicates that ZnO nanofibers annealed at 650°C show an excellent photocatalytic activity. © 2014 Wiley Periodicals, Inc. J. Appl. Polym. Sci. **2015**, *132*, 41627.

KEYWORDS: catalysts; electrospinning; morphology; nanostructured polymers

Received 3 June 2014; accepted 10 October 2014

DOI: 10.1002/app.41627

INTRODUCTION

Nanostructured semiconducting metal oxides are being widely utilized in the fields of solar energy conversion, sensors, catalysis and various electronic nanodevice due to their unique optical, electronic, and photoactive properties.[1–4] Zinc oxide (ZnO), a multifunctional semiconductor metal oxide, has stimulated an extensive range of research attention. With the development of nanotechnology, the structures with special shapes and dimensions have been prepared for nanocrystalline ZnO in the form of nanorods, nanoflowers, nanowires, and nanofibers.[5] Among anisotropic structures, zinc oxide nanofibers have exhibited a variety of practical applications in many advanced fields such as photocatalysis,[6] gas sensors,[7] field emission emitters,[1] visible light detectors,[8] and optical devices.[9] It is reported that the properties of nanomaterial mainly depend on its structure and morphology. Tinier nanomaterials are usually more active and exhibit more enhanced selectivity.[10] Thus, making efforts to fabricate nanomaterials with well–defined morphology is promising to acquire unique property and accomplish specific application.[11] In some cases, nanostructured ZnO with multiple branch morphology probably possesses high specific surface area, which can enhance their excellent performance in photocatalytic activity. Therefore, to further penetrate into its applications, new special structures are required.

In recent study, many efforts have been employed for the synthesis of one–dimensional ZnO, which include the template–induced method,[12] the microemulsion hydrothermal process,[13] the metal–organic chemical vapor deposition,[14] and wet chemical method,[15] and so on. However, the principal drawbacks of these synthesis approaches are attributed to the multiple and complicated processing steps. In particular, electrospinning technique, a versatile and mature method, has been exploited to manufacture nanofibers of polymers ranging from tens of nanometers to several micrometers and related materials into one–dimensional structural nanofibers with controllable diameters, compositions and porosities.[16,17] In terms of the fabrication and integration processes for metal oxide nanofibers, this method possesses the advantage of facile composition control. Thus far some reports pointed out that nanomaterial ZnO has been extensively applied to degrade nonbiodegradable dyes through photocatalytical routes.[18] It is mainly attribute to their high photosensitivity, stability and large band gap.[9] Therefore, the majority of researches have focused on enhancing degradation efficiency of organic pollutants by combining inorganic

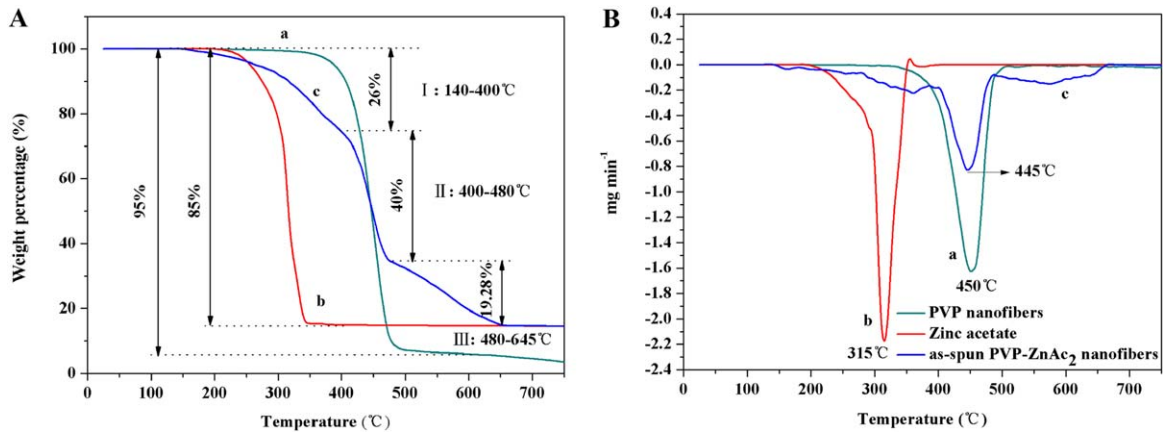

Figure 1. TG–DTG curves of thermal decomposition of (a) pure PVP nanofibers; (b) zinc acetate, and (c) as-spun PVP−$ZnAc_2$ composite nanofibers. [Color figure can be viewed in the online issue, which is available at wileyonlinelibrary.com.]

materials with polymers to realize complementary and synergetic behaviors.[18]

In this work, we described the fabrication of ZnO nanofibers with a peculiar dendritic morphology by electrospinning and subsequent calcination. The thermal property of the ZnO was evaluated using Thermo–Gravimetric Analysis (TGA). The surface morphology and dimension of ZnO nanofibers were observed by scanning electron microscope (SEM). X–ray diffraction (XRD), Fourier transform–Infrared radiation spectrometer (FTIR) and Photoluminescence (PL) spectroscopy measurements identified that the sample was pure ZnO with hexagonal wurtzite structure. Whereafter, comparison of the photocatalytic performance of the ZnO nanofibers annealed at 400 and 650°C (we call ZnO–400 and ZnO–650 in this article) was carried out.

EXPERIMENTAL

Chemicals and Materials

Zinc acetate A.R. [$Zn(CH_3COO)_2 \cdot 2H_2O$] was purchased from Beijing Chemical Works Fine Chemicals Reagent Company, Beijing, China. Polyvinylpyrrolidone (PVP) (M_w = 1,300,000, K88–96) was provided by Aladdin Reagent, Shanghai, China. The solvent methanol A.R. was produced by Beijing Chemical Works, Beijing, China. Methyl blue was produced by Research Institute of Guangfu Fine Chemical Engineering in Tianjin. All those chemical reagents were analytical grade, without further purification.

Preparation of Electrospun ZnO Nanofibers

Based on a typical procedure, zinc acetate (6 wt %) was dissolved in methanol solvent under magnetic stirring. When the solution became transparent after 2 h at room temperature, polyvinylpyrrolidone (PVP) (10 wt %) was added to the above solution. After continuous stirring for 5.5 h, precursor solution of PVP/zinc acetate/methanol was obtained. The homogenous eletrospinning solution was charily sucked into a glass syringe which was connected to a high-voltage supply (DW–P303–5AC HighVoltage (0∼30 KV), Dongwen High–voltage Power–supply Company, China). An aluminum foil with SiO_2/Si substrate placed on was used as the collector. The applied high voltage was held at 15.5 KV and the distance between the needle tip and the collector was maintained at 20 cm. Finally, a dense web of electrospun composite nanofibers was distributed uniformly over the collector. It was subsequently exposed to the air overnight for stabilization.

To obtain pure inorganic oxides, the PVP–$ZnAc_2$ composite nanofibers were respectively calcinated at 400 and 650°C in air with a heating rate of 5°C /min for 4 h.

Characterization

Thermal gravimetric analysis (TGA) was performed on a TG–DTG instrument (Beijing Hengjiu Instrument, Beijing, China) to determine the temperature of possible decomposition and crystallization of the nanofibers. Measurement was conducted from temperature of 25°C to 750°C, with a heating rate of 10°C/min under nitrogen gas. The surface morphology and dimension of ZnO nanofibers were observed under scanning electron microscope (SEM) (SHIMDZU SSX–550, Japan) equipped with energy dispersive X–ray analysis (EDX). Before testing, the ZnO nanofibers were sputter coated with gold using ETD–2000 auto sputter coater (Elaborate Technology Development, China) with a current of 4 mA for 2 min. Ground on the SEM images, diameter of nanofibers was measured using image visualization software Image J. The Brunauer–Emmett–Teller (BET) specific surface area of the nanofibers was investigated through nitrogen adsorption (Micromeritics, ASAP 2010). The samples were degassed at 200°C before the measurements. The crystalline structures of the PVP–$ZnAc_2$ composite and annealed ZnO nanofibers were identified by XRD. X–ray diffraction (XRD) analysis was obtained using a Siemens D5005 XRD diffractometer in 2θ region of 20–80° with Cu Kα radiation. Fourier transform–Infrared radiation (FTIR) spectrometer (SHIMDZU, 1.50SU1, Japan) was used to identify the vibration in functional groups presented in the samples. The spectra were obtained with 20 scans per sample ranging from 4000 to 400 cm^{-1}. The Photoluminescence (PL) spectra of the ZnO nanofibers was measured by using a Fluorescence

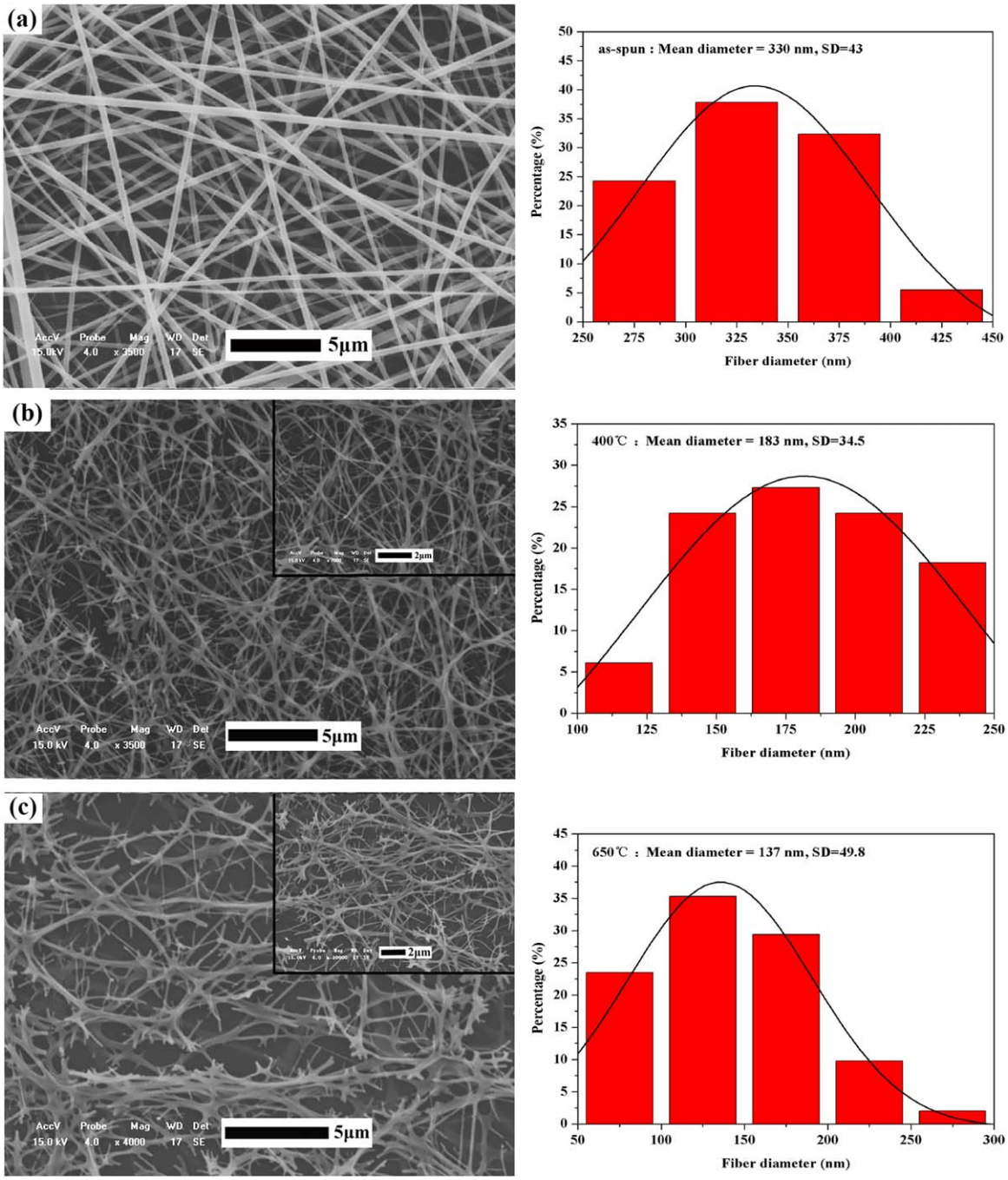

Figure 2. SEM micrographs of (a) as - spun PVP - $ZnAc_2$ composite nanofibers; after annealing at different temperature. (b) 400°C; (c) 650°C; and their corresponding diameter distribution. [Color figure can be viewed in the online issue, which is available at wileyonlinelibrary.com.]

Spectrophotometer (Jobin Yvon FluoroMax–4) equipped with a 150 W xenon lamp as the excitation source.

Photocatalytic Activity Measurement

Methyl blue has been vastly used as a model compound to indicate photocatalytic activity, which is primarily attributed to their frequent occurrence in industrial waste discharge. The photocatalytic activities of the as–prepared samples (ZnO–400 and ZnO–650 nanofibers) were evaluated by the decomposition of methyl blue under ultraviolet light irradiation. An aqueous solution of methyl blue (10 mL, 35 mg/L) was placed in a vessel, and 4 mg photocatalysts (ZnO–400 and ZnO–650) were added, respectively. Then the solution was exposed to an ultraviolet (UV) – radiation lamp (UV–8, 12W, 365 nm). The suspensions were magnetically stirred at ambient temperature to ensure that all of catalysts were contacted with the dye solution. At given time intervals, a few milliliters of solution were drawn from the mixture and centrifuged to separate the nanofibers. Then the solution was loaded in a UV–vis spectrophotometer (Jinghua 723 PC, China). The degradation efficiency of methyl

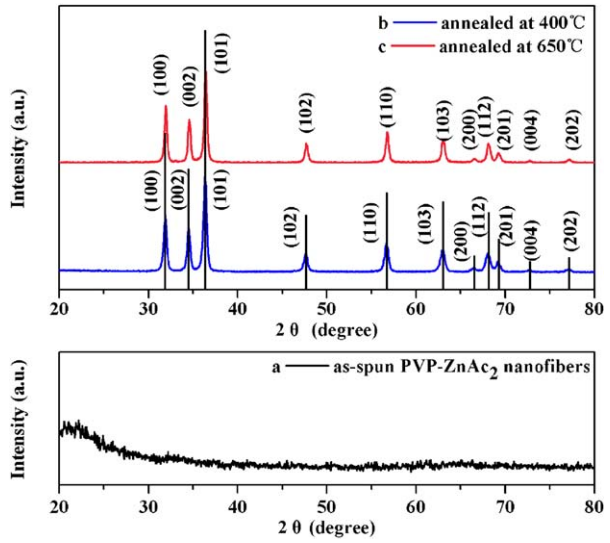

Figure 3. XRD patterns of (a) as - spun PVP - $ZnAc_2$ composite nanofibers and after annealing at different temperature. (b) 400°C; (c) 650°C. [Color figure can be viewed in the online issue, which is available at wileyonlinelibrary.com.]

blue was monitored by comparing the characteristic absorption intensity of the methyl blue solution at 628 nm at different time with that of the original methyl blue solution.

RESULTS AND DISCUSSION

Thermal Analysis of the PVP–$ZnAc_2$ Composite Nanofibers

TGA curve and corresponding DTG profile of the raw material and precursor PVP–$ZnAc_2$ composite nanofibers were shown in Figure 1. Initially, Figure 1B (a) revealed that the major weight loss of pure PVP nanofibers occurred at 450°C. This was consistent with nearly 95% mass loss in the range of 200–600°C [Figure 1A (a)], which was corresponded to the decomposition of the polymer main chain. Figure 1 A (b) presented almost 85% total weight loss from 200 to 350°C, associating with the decomposition of the CH_3COO group of zinc acetate.[17] Figure 1A (c) showed the thermal behavior of the PVP–$ZnAc_2$ composite nanofibers, which forecasted that most of the organic belonged to PVP, zinc acetate and other volatiles were completely decomposed before 645°C. It was found that the PVP–$ZnAc_2$ composite nanofibers exhibited a three–step thermogram, with a total weight loss of 85.28%. Below 400°C (occured at 300°C), there was a 26% weight loss; between 400 and 480°C, there was a 40% weight loss; and finally, 19.28% weight loss existed in the temperature range of 480–645°C. The first step was mainly attributed to the decomposition of acetate which showed dramatic weight loss approximate at 315°C [Figure 1B (b)], the degradation of PVP along with the release of small hydrocarbon molecules and others volatile solvent.[19] The second stage, in which the significant weight loss occurred at 445°C [Figure 1B (c)], was resulted from the continued decomposition of zinc acetate and release of the oxidation of carbon from PVP.[20] The third stage was related to the entirely removal of the organic constituents in the nanofibers. Compared with the complete weight loss of pure PVP nanofibers at ~600°C, the PVP–$ZnAc_2$ composite nanofibers were degraded at 650°C. Such high decomposition temperature might be attributed to the interaction between the PVP and ZnO materials, which led to high chain compactness.[21] After 645°C, the TGA curve was gentle, manifesting the formation of pure inorganic oxide.

Morphology and Diameter Distribution of the Nanofibers

Exemplary scanning electron microscope (SEM) micrographs of the PVP–$ZnAc_2$ composite nanofibers before and after calcination were depicted in Figure 2. Figure 2(a) revealed that the as–spun composite nanofibers appeared to be relatively smooth and uniform in terms of diameter due to the polymeric property or amorphous nature of zinc oxide PVP composite.[22,23] After Gaussian fitting and statistic, the mean diameter was 330 nm and the uniformity was above 71%. As shown in Figure 2(b), the ZnO–400 microstructure had a tendency of dendritic structure, and the diameter of the dendritic branch was ~183 nm which was markedly shrank. The shrinkage of the fiber diameter was ascribed to the removal of the organic components from the nanofibers and the crystallization of ZnO phase during the calcined process.[24] When the PVP–$ZnAc_2$ composite nanofibers calcined at 650°C [Figure 2(c)], the dendritic branch structure was obvious. The peculiar morphology was different from the previously reported ZnO nanofibers.[5,25] It was observed that each dendritic branch was constituted of a long main trunk and the ZnO dendrite branch interconnected with each other. This might be because that with the temperature increased which leading to the thermal instability, part of the nanofibers were fractured. After statistics, the diameter of ZnO dendrite branch was about 137 nm. The BET surface areas of ZnO–400 and ZnO–650 nanofibers were 3.6836 m^2/g and 5.8688 m^2/g, respectively. Obviously, the higher surface area of ZnO–650 nanofibers was tightly related with the dendritic branch structure. Since the oblique dendritic branch was elongated, the prepared ZnO–650 fibers could be a promising photocatalyst application for organic dyes degradation where surface area played an important role in determining their performance.

Structure Inspections

XRD Analysis. Figure 3 showed the XRD patterns of the as–spun PVP–$ZnAc_2$ composite nanofibers and ZnO nanofibers as a function of annealing different temperature. As shown in Figure 3(a), it was observed clearly that the PVP–$ZnAc_2$ composite nanofibers were amorphous in nature, which confirmed that the nanofibers were no obvious characteristic peaks. But a low intensity broad peak showed at around 21°, which was attributed to the amorphous nature of PVP.[26] When the PVP–$ZnAc_2$ composite nanofibers annealed at 400°C [Figure 3(b)], poor

Table I. Crystallite Size Along Main Diffraction Planes for ZnO Nanofibers Annealed at Different Temperatures

	Crystallite size (in nm) along diffraction planes		
Annealing temperature (°C)	(100)	(002)	(101)
400	22.1	23.3	21.7
650	25.8	27.1	24.6

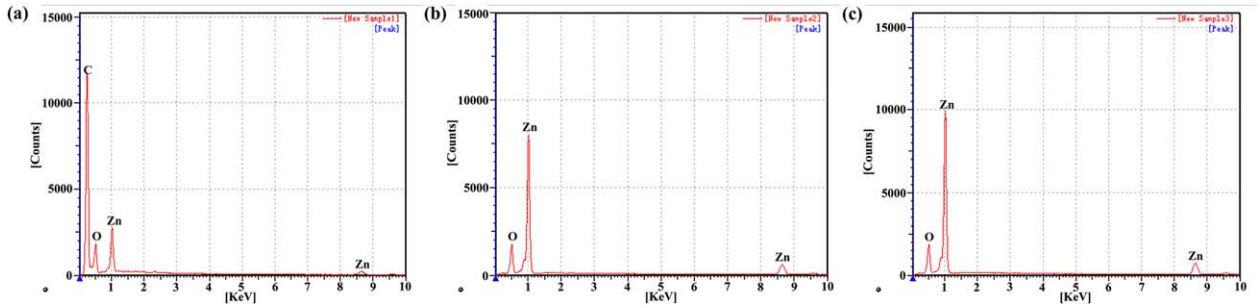

Figure 4. EDX spectroscopy of (a) as - spun PVP - $ZnAc_2$ composite nanofibers; (b) ZnO - 400 nanofibers; (c) ZnO - 650 nanofibers. [Color figure can be viewed in the online issue, which is available at wileyonlinelibrary.com.]

crystallinity can be seen. With the annealing temperature increased [Figure 3(c)], the peak became sharper and narrower. That was to say, the high temperature contributed to the formation of ZnO crystal. The crystallite size of the ZnO nanofibers was calculated through Scherrer's Equation.[27,28] As below:

$$D = {}^{K\lambda}/_{(\beta\cos\theta)} \quad (1)$$

Where D was the crystallite size, K was a Scherrer's constant ($K = 0.89$), θ was the angle of diffraction, wavelength of the X-ray used was $\lambda = 1.54$ Å, β was full width at half maximum of main peak. The crystallite size along main diffraction planes for ZnO nanofibers annealed at different temperatures were summarized in Table I. From the table, we observed that with increasing the annealing temperature, the main diffraction planes for ZnO crystallite size obviously increased. When the PVP–$ZnAc_2$ composite nanofibers annealed at 650°C, the peak belonging to PVP was disappeared. Figure 3(c) showed eleven main reflection peaks corresponding to (100), (002), (101), (102), (110), (103), (200), (112), (201), (004), and (202) planes at 31.936°, 34.584°, 36.390°, 47.673°, 56.778°, 63.024°, 66.508°, 68.072°, 69.209°, 72.739°, and 77.132°, respectively. All the diffraction peaks indicated the typical hexagonal wurtzite structure of zinc oxide, which were consistent with the values in the standard card JCPDS date 75–0576. The results of XRD patterns further confirmed that the calcination temperature of 650°C was sufficient to remove PVP completely which was corresponding to the TG curve.

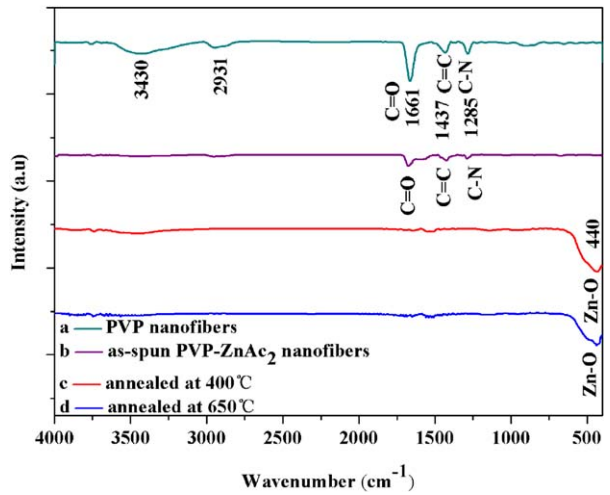

Figure 5. FTIR spectra of (a) pure PVP nanofibers; (b) as - spun PVP - $ZnAc_2$ composite nanofibers and after annealing at different temperature. (c) 400°C; (d) 650°C. [Color figure can be viewed in the online issue, which is available at wileyonlinelibrary.com.]

EDX Analysis

To further understand the chemical composition of the obtained nanofibers, Energy–dispersive X–ray (EDX) analysis was carried out. As shown in Figure 4(a), the EDX spectrum revealed the presence of carbon, oxygen and zinc in the as–spun PVP–$ZnAc_2$ composite nanofibers. Therein, the carbon peak mainly originated from the polymer. After annealing at 400 and 650°C, which were shown in Figure 4(b,c), only Zn and O atoms were observed. It demonstrated that the obtained nanofibers were indeed pure ZnO, which further supported the XRD results.

FTIR Spectra Analysis

FTIR spectrum was also performed to identify the structure of the obtained nanofibers, which was shown in Figure 5. For the spectra of pure PVP nanofibers [Figure 5(a)], a series of absorption peaks at around 1000 and 4000 cm^{-1} was observed. Therein, the peaks located at 2931, 1437, and 1285 cm^{-1} were corresponding to CH_2 unsymmetrical stretching vibration, C=C stretching vibration and C=N stretching vibration band, respectively.[29,30] Furthermore, the strong absorption peak centered at 1661 cm^{-1} was attributed to C=O stretching vibration. Notably, the broad band at about 3430 cm^{-1} was assigned to the

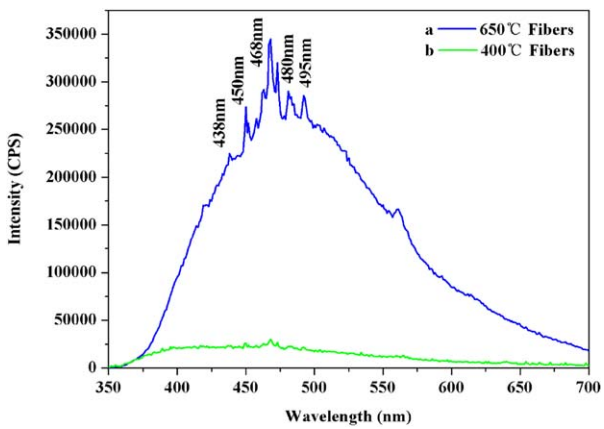

Figure 6. Photoluminescence spectra of (a) ZnO - 650 fibers; (b) ZnO - 400 fibers. [Color figure can be viewed in the online issue, which is available at wileyonlinelibrary.com.]

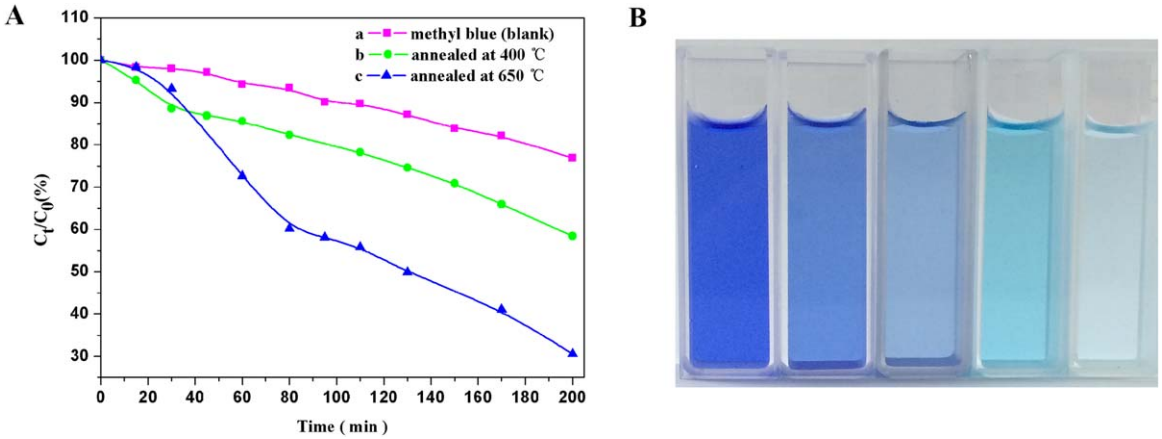

Figure 7. (A) Photocatalytic degradation of methyl blue concentration changes as a function of irradiation times after added different photocatalysis. (a) without any catalyst; (b) ZnO - 400 fibers; (c) ZnO - 650 fibers. (B) Photographic image of the color change of the methyl blue using ZnO - 650 catalyst with different times of UV irradiation. [Color figure can be viewed in the online issue, which is available at wileyonlinelibrary.com.]

O—H stretching vibration of water,[31] which may be molecularly absorbed on PVP nanofibers. Figure 5(b) depicted the spectrum of the PVP–$ZnAc_2$ composite nanofibers and it was seemed the same as Figure 5(a). This indicated that most of the ZnO precursor was embedded in the PVP chain.[32] Moreover, the strong absorption peak of the carbonyl group stretching vibration was shifted to 1670 cm^{-1} in the PVP–$ZnAc_2$ composite nanofibers. It was because that the oxygen atoms of the polypyrrolidone units of PVP were interacting with the inorganic nanoparticles which might induce a shift in FTIR periodicity on account of the metal atoms received an electron pair of the carbonyl oxygen.[33–35] When the nanofibers were annealed at 400°C and 650°C [Figure 5(c,d)], the representative absorption peaks of PVP disappeared gradually and a new intense broadband at 440 cm^{-1} appeared. This band corresponded to the Zn—O vibration of hexagonal ZnO.[36] FTIR analysis demonstrated that after high temperature treatment, polymer was decomposed thoroughly and pure inorganic oxides were produced. The results accorded well with XRD and EDX analysis.

Photoluminescence Spectra of ZnO

Photoluminescence spectra is an available way to analyze electronic structure, optical, and photochemical properties of semiconductor material, by reflecting some significant informations such as surface defects and oxygen vacancies.[37]

The photoluminescence spectra of the prepared ZnO fibers annealed at different temperatures with an excited wavelength of 320 nm was shown in Figure 6. The emission can exhibit a strong and wide broadband in the range of 430–580 nm, typically there were emission bands in the visible region. Specially, the main intense emission peak centered at the blue and blue–green bands.

It was known that the visible luminescence mainly originated from defect states such as Zn interstitials and oxygen vacancies, resulting from the radiative recombination of photogenerated holes (h_{VB}^{+}) with electrons capturing the oxygen vacancy.[38,39] In general, oxygen vacancies can act as luminescence center.[8] As shown in Figure 6(a), it had three strong blue light emission peaks in the range of 438–470 nm, which was associated with oxygen vacancies.[40,41] The blue–green light emission at around 480–500 nm was known to be related to radiative defect, among that 480 nm was ascribed to bound excitons, especially singly ionized oxygen vacancy.[37] The excitonic photoluminescence intensity of ZnO distinctly reduced with the decrease in the temperature. In other words, the peak intensity of ZnO was lower at 400°C. It might be attributed to the ZnO–400 fibers poor crystallinity, consistent with the XRD result, which showed little luminescence property. Hence the stronger photoluminescence intensity was determined by the higher content of surface oxygen vacancies in the ZnO crystal, probably lead to the higher photocatalytic activity,[11,37] reflected in Figure 7.

Properties of Photocatalysis

To identify the photocatalytic performance of the ZnO nanofibers under different temperature conditions, the decolorization of methyl blue in an aqueous solution was investigated under UV light irradiation. From Figure 7(A), after UV irradiation for 200 min, 23% of methyl blue [Figure 7A (a)] can be photodegraded by itself. In comparison, the observed rate of methyl blue photodegradation using ZnO–400 and ZnO–650 nanofibers had reached to 19% and 47% as compared with methyl blue, respectively. This result was consistented with the photoluminescence emission spectra. Overall, Figure 7A(b,c) showed that the initial degradation efficiency of methyl blue (up to 30 min) with ZnO–400 fibers was higher than the premier degradation efficiency of ZnO–650 fibers under identical conditions of UV light exposure. But after 30 min, the ZnO–650 nanofibers suffered from a significant decrease in photocatalytic activity. The poor photocatalytic performance of ZnO–400 nanofibers was ascribed to light filtering and the fewer photogenerated charge carriers.[8] Notably, the reason for the higher photocatalytic activity of ZnO–650 can be explained in two aspects: on the one hand, in reasonable agreement with the result obtained from the XRD analysis, the ZnO calcined at 650°C was almost completely crystalline. Thus it had better optical absorption of UV light and the photoinduced dissolution.[42] On the other hand, from Figure 2(c), ZnO–650 nanofibers possessed unique dendritic structure and high special surface area. This result might be

favorable to the reaction with methyl blue, leading to a good photocatalytic property. Figure 7(B) showed a photographic image of the methyl blue using ZnO–650 photocatalyst, in which we can see a series of color change at different UV irradiation time. It made clear that the distinct blue color of initiating solution gradually became transparent and colorless. That was further confirmed the completion of the photodegradation process.

CONCLUSIONS

In conclusion, hexagonal wurtzite ZnO nanofibers with special dendritic structure was successfully synthesized through electrospinning and subsequent calcination techniques. The as–spun PVP–$ZnAc_2$ composite nanofibers had smooth surfaces with diamater of 330 nm. The calcination process at high temperature for 4 h induced the formation of ZnO nanofibers and resulted in a peculiar dendritic structure with the branch diameter ranging from 100 nm to 200 nm. The photoluminescence spectra had confirmed that the ZnO nanofibers exhibited a broad visible emission mainly concentrate on the blue and blue–green emission bands. Furthermore, it indicated the existence of surface oxygen vacancies in the ZnO crystallines, which probably related with photocatalytic activity. Methyl blue was used to evaluate the photocatalytic activity of the ZnO nanofibers. The photocatalytic performance of the ZnO nanofibers annealed at 400 and 650°C was investigated. The results manifested that the particular ZnO–650 with dendritic structure exhibited superior photocatalytic activity. Further, we believe that the ZnO–650 nanofibers can be considered as a promising photocatalyst for dyes treatment.

ACKNOWLEDGMENTS

The authors are grateful to the Basic Research Program of Jilin Provincial Science and Technology Department (20130102040JC) and Changchun Science and Technology Project (13NK01) for their financial support.

REFERENCES

1. Moon, J.; Lee, S.-J.; Park, J.-A.; Zyung, T. *Electrochem. Solid-State Lett.* **2009**, *12*, K63.
2. Ye, S.; Zhang, D.; Liu, H.; Zhou, J. *J. Appl. Polym. Sci.* **2011**, *121*, 1757.
3. Kundu, S. *Colloids Surf. A: Physicochem. Eng. Aspects.* **2014**, *446*, 199.
4. Kanjwal, M. A.; Sheikh, F. A.; Barakat, N. A. M.; Chronakis, I. S.; Kim, H. Y. *Appl. Surf. Sci.* **2011**, *257*, 7975.
5. Yu, X.; Song, F.; Zhai, B.; Zheng, C.; Wang, Y. *Phys. E: Low-Dimensional Syst. Nanostruct.* **2013**, *52*, 92.
6. Xu, L.; Hu, Y.-L.; Pelligra, C.; Chen, C.-H.; Jin, L.; Huang, H.; Sithambaram, S.; Aindow, M.; Joesten, R.; Suib, S. L. *Chem. Mater.* **2009**, *21*, 2875.
7. Masuda, Y.; Kato, K. *Crystal Growth Des.* **2009**, *9*, 3083.
8. An, S.; Joshi, B. N.; Lee, M. W.; Kim, N. Y.; Yoon, S. S. *Appl. Surf. Sci.* **2014**, *294*, 24.
9. Sakthivel, S.; Neppolian, B.; Shankar, M. V.; Arabindoo, B.; Palanichamy, M.; Murugesan, V. *Solar Energy Mater. Solar Cells* **2003**, *77*, 65.
10. Bian, S.-W.; Mudunkotuwa, I. A.; Rupasinghe, T.; Grassian, V. H. *Langmuir* **2011**, *27*, 6059.
11. Li, C.; Hu, R.; Zhou, T.; Wu, H.; Song, K.; Liu, X.; Wang, R. *Mater. Lett.* **2014**, *124*, 81.
12. Park, W. I.; D. H. K., Jung, S.-W.; Gyu-Chul, Y. *Appl. Phys. Lett.* **2002**, *80*, 4232.
13. Colón, G.; Hidalgo, M. C.; Navío, J. A.; Pulido Melián, E.; González Díaz, O.; Doña Rodríguez, J. M. *Appl. Catalysis B: Environ.* **2008**, *83*, 30.
14. Falyouni, F.; Benmamas, L.; Thiandoume, C.; Barjon, J.; Lusson, A.; Galtier, P.; Sallet, V. *J. Vacuum Sci. Technol. B: Microelectron. Nanometer Struct.* **2009**, *27*, 1662.
15. Jesuvathy Sornalatha, D.; Murugakoothan, P. *Mater. Lett.* **2014**, *124*, 219.
16. Panthi, G.; Barakat, N. A. M.; Al-Deyab, S. S.; El-Newehy, M.; Pandeya, D. R.; Kim, H. Y. *J. Appl. Polym. Sci.* **2013**, *127*, 2025.
17. Zhang, Z.; Li, X.; Wang, C.; Wei, L.; Liu, Y.; Shao, C. *J. Phys. Chem. C* **2009**, *113*, 19397.
18. Eskizeybek, V.; Sarı, F.; Gülce, H.; Gülce, A.; Avcı, A. *Appl. Catalysis B: Environ.* **2012**, *119*, 197.
19. Bianco, G.; Soldi, M. S.; Pinheiro, E. A.; Pires, A. T. N.; Gehlen, M. H.; Soldi, V. *Polym. Degrad. Stabil.* **2003**, *80*, 567.
20. Zhang, Y.; Li, J.; Li, Q.; Zhu, L.; Liu, X.; Zhong, X.; Meng, J.; Cao, X. *Scripta Materialia.* **2007**, *56*, 409.
21. Mali, S. S.; Kim, H.; Jang, W. Y.; Park, H. S.; Patil, P. S.; Hong, C. K. *ACS Sustainable Chem. Eng.* **2013**, *1*, 1207.
22. Wei, S.; Zhou, M.; Du, W. *Sens. Actuators B Chem.* **2011**, *160*, 753.
23. Yuh, J.; Nino, J. C.; Sigmund, W. M. *Mater. Lett.* **2005**, *59*, 3645.
24. Park, J.-A.; Moon, J.; Lee, S.-J.; Lim, S.-C.; Zyung, T. *Curr. Appl. Phys.* **2009**, *9*, S210.
25. Katoch, A.; Sun, G.-J.; Choi, S.-W.; Byun, J.-H.; Kim, S. S. *Sens. Actuators B Chem.* **2013**, *185*, 411.
26. Kumar, K. K.; Ravi, M.; Pavani, Y.; Bhavani, S.; Sharma, A. K.; Narasimha Rao, V. V. R. *J. Membr. Sci.* **2014**, *454*, 200.
27. Lin, D.; Wu, H.; Zhang, R.; Pan, W. *Chem. Mater.* **2009**, *21*, 3479.
28. Guo, D.; Sato, K.; Hibino, S.; Takeuchi, T.; Bessho, H.; Kato, K. *Thin Solid Films* **2014**, *550*, 250.
29. Zhang, Z.; Shao, C.; Gao, F.; Li, X.; Liu, Y. *J. Colloid Interface Sci.* **2010**, *347*, 215.
30. Sui, X.; Liu, Y.; Shao, C.; Liu, Y.; Xu, C. *Chem. Phys. Lett.* **2006**, *424*, 340.
31. Li, Q.; Li, T.; Wu, J. *J. Phys. Chem. B* **2000**, *104*, 9011.
32. Liu, M.; Cheng, Z.; Yan, J.; Qiang, L.; Ru, X.; Liu, F.; Ding, D.; Li, J. *J. Appl. Polym. Sci.* **2013**, *128*, 1095.
33. Lu, X.; Zhao, Y.; Wang, C. *Adv. Mater.* **2005**, *17*, 2485.

34. Lu, X.; Zhao, Y.; Wang, C.; Wei, Y. *Macromol. Rapid Commun.* **2005**, *26*, 1325.

35. Bai, J.; Li, Y.; Zhang, C.; Liang, X.; Yang, Q. *Colloids Surf. A* **2008**, *329*, 165.

36. Xiong, G.; Pal, U.; Serrano, J. G.; Ucer, K. B.; Williams, R. T. *Phys. Status Solidi (c)* **2006**, *3*, 3577.

37. Liqiang, J.; Yichun, Q.; Baiqi, W.; Shudan, L.; Baojiang, J.; Libin, Y.; Wei, F.; Honggang, F.; Jiazhong, S. *Solar Energy Mater. Solar Cells* **2006**, *90*, 1773.

38. Liu, Y.; Kang, Z. H.; Chen, Z. H.; Shafiq, I.; Zapien, J. A.; Bello, I.; Zhang, W. J.; Lee, S. T. *Crystal Growth Des.* **2009**, *9*, 3222.

39. Vanheusden, K.; Seager, C. H.; Warren, W. L.; Tallant, D. R.; Voigt, J. A. *Appl. Phys. Lett.* **1996**, *68*, 403.

40. Zhu, Z.; Yang, D.; Liu, H. *Adv. Powder Technol.* **2011**, *22*, 493.

41. Tapas Kumar Kundu, N. K., Puspendu Barik, Satyajit Saha, International Journal of Soft Computing and Engineering. 2011, 1.

42. Fu, H.; Xu, T.; Zhu, S.; Zhu, Y. *Environ. Sci. Technol.* **2008**, *42*, 8064.